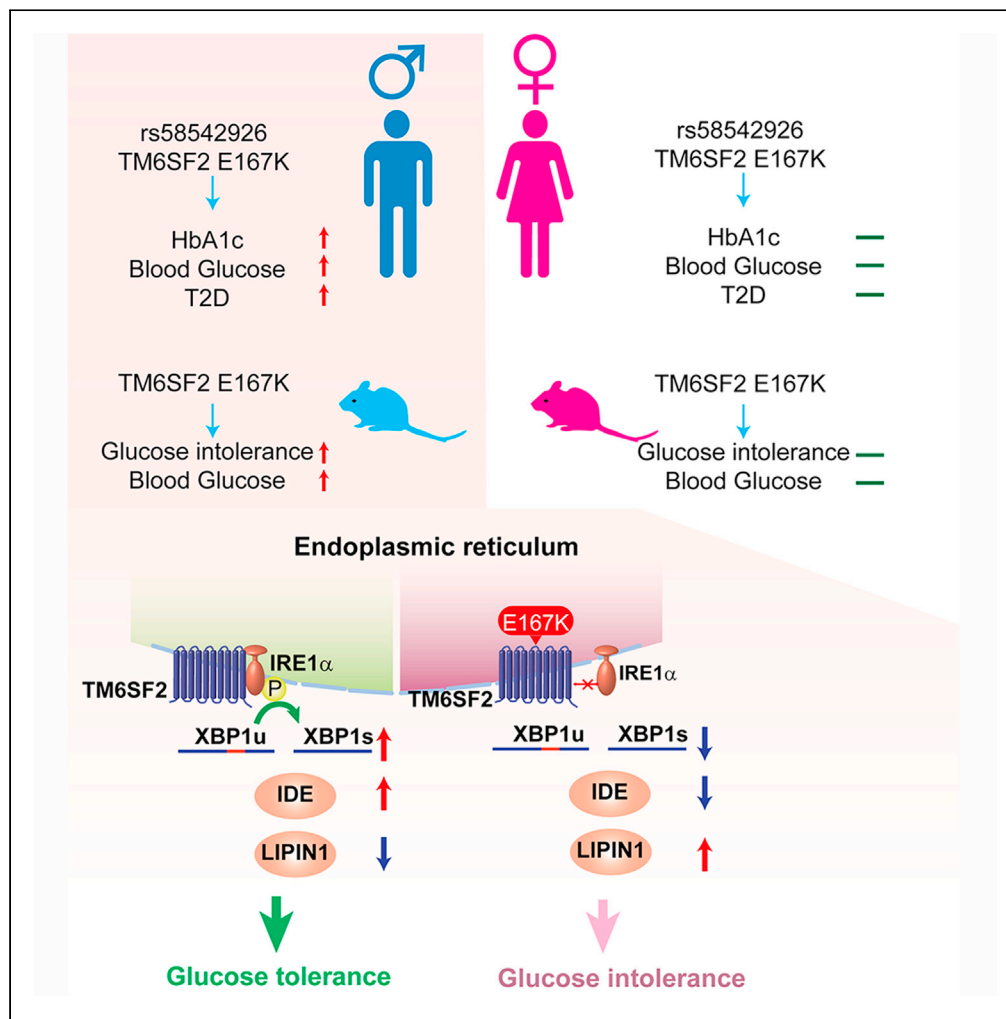## Article

Type 2 diabetes sex-specific effects associated with E167K coding variant in *TM6SF2*

Yanbo Fan,
Brooke N.
Wolford,
Haocheng Lu, ...,
Kezhong Zhang,
Cristen J. Willer, Y.
Eugene Chen

fanyb@ucmail.uc.edu (Y.F.)
cristen@umich.edu (C.J.W.)
echenum@umich.edu (Y.E.C.)

Highlights
The *TM6SF2* E167K
variant is significantly
associated with T2D,
primarily in males

Male, but not female,
Tm6sf2 KI mice exhibited
impaired glucose
tolerance

IRE1α signaling is
attenuated in the liver of
male *Tm6sf2* KI mice

IDE and LIPIN1 were
dysregulated in the liver of
male KI mice but not the
females

Article

Type 2 diabetes sex-specific effects associated with E167K coding variant in *TM6SF2*

Yanbo Fan,[1,2,13,15,*] Brooke N. Wolford,[3,13] Haocheng Lu,[1,13] Wenying Liang,[1] Jinjian Sun,[1] Wei Zhou,[3] Oren Rom,[1,4] Anubha Mahajan,[5,14] Ida Surakka,[1] Sarah E. Graham,[1] Zhipeng Liu,[6] Hyunbae Kim,[7] Shweta Ramdas,[8] Lars G. Fritsche,[9] Jonas B. Nielsen,[1] Maiken Elvestad Gabrielsen,[10] Kristian Hveem,[10] Dongshan Yang,[1] Jun Song,[1] Minerva T. Garcia-Barrio,[1] Jifeng Zhang,[1] Wanqing Liu,[11] Kezhong Zhang,[7] Cristen J. Willer,[1,3,12,15,*] and Y. Eugene Chen[1,15,16,*]

SUMMARY

The rs58542926C >T (E167K) variant of the transmembrane 6 superfamily member 2 gene (*TM6SF2*) is associated with increased risks for nonalcoholic fatty liver disease (NAFLD) and type 2 diabetes (T2D). Nevertheless, the role of the *TM6SF2* rs58542926 variant in glucose metabolism is poorly understood. We performed a sex-stratified analysis of the association between the rs58542926C >T variant and T2D in multiple cohorts. The E167K variant was significantly associated with T2D, especially in males. Using an E167K knockin (KI) mouse model, we found that male but not the female KI mice exhibited impaired glucose tolerance. As an ER membrane protein, TM6SF2 was found to interact with inositol-requiring enzyme 1 α (IRE1α), a primary ER stress sensor. The male *Tm6sf2* KI mice exhibited impaired IRE1α signaling in the liver. In conclusion, the E167K variant of TM6SF2 is associated with glucose intolerance primarily in males, both in humans and mice.

INTRODUCTION

Metabolic diseases including nonalcoholic fatty liver disease (NAFLD), type 2 diabetes (T2D), and obesity coexist regularly. NAFLD has been recognized to increase the incidence of T2D, and in turn, T2D aggravates NAFLD, including steatohepatitis, cirrhosis, and hepatocellular carcinoma (Firneisz, 2014; Lang et al., 2019). Recent studies focusing on the genetic basis of metabolic diseases identified the association of specific gene variants with lipid and glucose traits, thereby leading to these diseases (Lang et al., 2019).

In humans, transmembrane 6 superfamily member 2 (*TM6SF2*) is highly expressed in the small intestine and liver (Kozlitina et al., 2014; Mahdessian et al., 2014). Genetic and biological studies reported different outcomes of the *TM6SF2* coding variant in lipid metabolism and potential consequences for coronary artery disease and liver disease (Kahali et al., 2015). The minor allele at a nonsynonymous variant (rs58542926, c.449C >T, encoding p. E167K) in the human *TM6SF2* gene is associated with lower levels of blood total cholesterol (TC) and reduced risk of myocardial infarction and cardiovascular disease (Dongiovanni et al., 2015; Holmen et al., 2014; Sookoian et al., 2015). In contrast, carriers of the minor allele (encoding lysine at codon 167) have an increased risk for NAFLD, steatosis, fibrosis, and cirrhosis (Kozlitina et al., 2014; Liu et al., 2014; Mahdessian et al., 2014; Sookoian et al., 2015). These phenotypes were recapitulated in previously reported animal models. *Tm6sf2*-deficient mice exhibited a decrease in TC (Fan et al., 2016) but an increase in hepatic steatosis (Smagris et al., 2016). In a zebrafish model, Tm6sf2 deficiency increased lipid accumulation in the small intestine in response to dietary lipids (O'Hare et al., 2017).

Although genetic studies suggest that the T allele at rs58542926 is positively associated with T2D (Kim et al., 2017; Liu et al., 2017), the biological function of *TM6SF2* in diabetes and glucose metabolism needs to be further elucidated. Such studies could lead to the development of a feasible therapeutic strategy harnessing the protective effects, while minimizing the adverse effects by targeting *TM6SF2*. In the present study, we aimed to explore the poorly understood role of the TM6SF2 rs58542926 variant in glucose

[1]Cardiovascular Center, Department of Internal Medicine, University of Michigan Medical Center, NCRC Bldg 26, Rm 361S, 2800 Plymouth Road, Ann Arbor, MI 48109, USA

[2]Department of Cancer Biology, University of Cincinnati College of Medicine, Vontz Center, 3125 Eden Avenue, Cincinnati, OH45267, USA

[3]Department of Computational Medicine and Bioinformatics, University of Michigan, Ann Arbor, MI48109, USA

[4]Department of Pathology and Translational Pathobiology, Louisiana State University Health Sciences Center-Shreveport, Shreveport, LA71103, USA

[5]Wellcome Centre for Human Genetics, University of Oxford, Oxford, UK

[6]Department of Medicinal Chemistry and Molecular Pharmacology, College of Pharmacy, Purdue University, West Lafayette, IN, USA

[7]Center for Molecular Medicine and Genetics, Wayne State University School of Medicine, Detroit, MI48201, USA

[8]Department of Genetics, University of Pennsylvania, Philadelphia, PA, USA

[9]Department of Biostatistics, University of Michigan School of Public Health, Ann Arbor, MI, USA

[10]K.G. Jebsen Center for Genetic Epidemiology, Department of Public Health and Nursing, Faculty of Medicine and Health Sciences, Norwegian
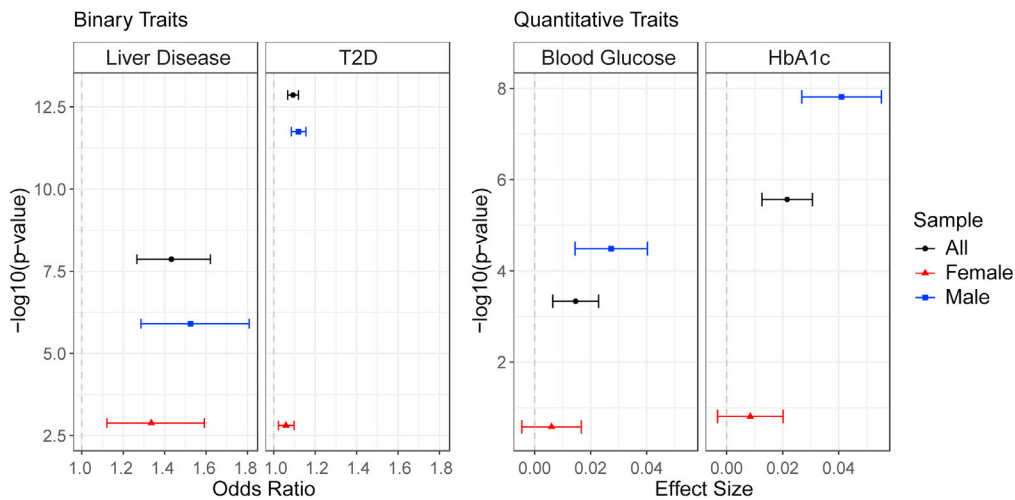
Figure 1. Inverse variance weighted fixed-effect meta-analysis of additive model association analysis at rs58542926

The single-variant association (see STAR Methods) for binary traits (chronic liver disease without alcoholic cirrhosis [liver disease] and type 2 diabetes [T2D]) and quantitative traits (blood glucose and HbA1c). Estimated effect sizes are shown as odds ratios for binary traits and estimated beta coefficients for quantitative traits with 95% confidence intervals. The null hypothesis of an odds ratio of 1 and beta coefficient of 0 is indicated by the vertical black line.

metabolism. We found that the T allele at rs58542926 is significantly associated with an increased incidence of T2D, primarily in males. Using a *Tm6sf2* KI mouse model, we demonstrated that the coding variant impairs glucose tolerance in males but not in females and investigated the underlying molecular mechanisms.

RESULTS

TM6SF2 E167K is associated with cardiometabolic diseases in humans

We studied the *TM6SF2* missense variant rs58542926-T through inverse variance weighted fixed-effects meta-analysis of single variant association results from two predominantly European ancestry cohorts—Trøndelag Health Study (HUNT, N = 69,635) and UK Biobank (UKB, N = 408,595). The rs58542926-T variant was found to be significantly associated with increased risk of chronic liver disease without alcoholic cirrhosis in males (odds ratio = 1.53, 95% CI [1.29,1.81], pvalue = 1.24×10^{-6}) and females (odds ratio = 1.33, 95% CI [1.12,1.59], pvalue = 1.31×10^{-3}) at Bonferroni corrected alpha = 0.00278 (Figure 1 and Table 1). In single variant association results from a large meta-analysis by the DIAGRAM consortium (effective N = 224,421) (Mahajan et al., 2018), the rs58542926-T variant was found to be significantly associated with T2D in males (odds ratio = 1.11, 95% CI [1.09,1.14], pvalue = 1.79×10^{-12}) and in females (odds ratio = 1.06, 95% CI [1.03,1.09], pvalue = 1.56×10^{-3}) (Figure 1 and Table 1). Of note, in a typical genome-wide association study with a genome-wide significance threshold of 5×10^{-8}, this variant would not have been reported as significant for females but would for males. The difference in this variant's effect size between males and females was found to be nominally significant (pvalue = 0.023) but does not meet the Bonferroni threshold for significance (Table 1).

Furthermore, we analyzed the association of rs58542926-T with traits related to glycemia, obesity, and lipids among a combination of UKB, HUNT, and the Genetic Investigation of Anthropometric Traits (GIANT) consortium (Tables 1 and S10). Using a Bonferroni significance threshold of 0.00278, our analysis revealed that the variant is significantly associated with increased blood glucose and Hb1Ac in males but not females (Figure 1 and Table 1). The missense variant is also significantly associated with decreased TC, triglycerides (TGs), and low-density lipoprotein cholesterol (LDL-c) in both males and females (Table 1). The difference in effect size between males and females was significantly different (pvalue < 0.00278) for HbA1C, TC, TG, and LDL. The sex-specific effect sizes were nominally significantly different (pvalue < 0.05) for blood glucose (Table 1). Collectively, the rs58542926-T variant is associated with increased risk of chronic nonalcoholic liver disease and T2D with related quantitative traits (blood glucose and Hb1Ac), demonstrating statistically significant differences in effect size between the sexes.

University of Science and Technology, NTNU, Trondheim, Norway

[11]Department of Pharmaceutical Sciences, Eugene Applebaum College of Pharmacy and Health Sciences, Wayne State University, Detroit, MI 48201, USA

[12]Department of Human Genetics, University of Michigan, Ann Arbor, MI, USA

[13]These authors contributed equally

[14]Present address: Genentech, 1 DNA Way, South San Francisco, CA 94080, USA

[15]Senior author

[16]Lead contact

*Correspondence: fanyb@ucmail.uc.edu (Y.F.), cristen@umich.edu (C.J.W.), echenum@umich.edu (Y.E.C.)

https://doi.org/10.1016/j.isci.2021.103196

Table 1. Single variant associations between rs58542926 and quantitative and binary traits in males and females in biobanks (UKB and HUNT) and consortia (GIANT and DIAGRAM)

Quantitative trait	Study	Females			Males			Difference in effect
		Beta (SE)	N	P	Beta (SE)	N	p-value	p-value
HbA1c	UKB + HUNT	0.008 (0.006)	211,545	0.16	0.041 (0.007)	179,942	1.54×10^{-8}	1.49×10^{-5}
Blood glucose	UKB + HUNT	0.006 (0.005)	226,793	0.26	0.027 (0.007)	196,310	3.29×10^{-5}	0.01
BMI	GIANT + UKB	−0.008 (0.006)	221,863	0.15	−0.002 (0.005)	262,817	0.67	0.43
WHR adjusted BMI	GIANT + UKB	0.014 (0.006)	221,804	0.01	0.027 (0.005)	262,759	8.75×10^{-8}	0.08
TC	UKB + HUNT	−0.11 (0.006)	247,079	6.69×10^{-74}	−0.20 (0.006)	211,499	1.43×10^{-220}	1.54×10^{-16}
TG	UKB + HUNT	−0.088 (0.006)	247,095	1.34×10^{-55}	−0.14 (0.006)	211,420	1.49×10^{-105}	7.64×10^{-4}
HDL	UKB + HUNT	−0.015 (0.006)	227,859	0.01	0.013 (0.006)	197,707	0.05	0.25
LDL	UKB + HUNT	−0.094 (0.006)	246,210	3.84×10^{-58}	−0.19 (0.006)	209,848	7.71×10^{-210}	3.03×10^{-18}
Binary trait	Study	Odds ratio (95% CI)	N	P	Odds ratio (95% CI)	N	p-value	Difference in effect p-value
T2D	DIAGRAM	1.06 (1.03,1.09)	96,460[a]	1.56×10^{-3}	1.11 (1.09, 1.14)	127,961[a]	1.79×10^{-12}	0.02
IHD	UKB + HUNT	0.99 (0.94, 1.03)	257,557	5.35×10^{-1}	0.94 (0.91, 0.98)	220,076	1.32×10^{-3}	0.12
Liver disease	UKB + HUNT	1.34 (1.12, 1.59)	254,076	1.31×10^{-3}	1.53 (1.29, 1.81)	216,884	1.24×10^{-6}	0.29
MI	UKB + HUNT	1.0036 (0.93,1.08)	250,127	9.89×10^{-1}	0.93 (0.89, 0.98)	207,523	8.55×10^{-3}	0.10

Hemoglobin A1c (HbA1c), United Kingdom Biobank (UKB), Nord-Trøndelag Health Study (HUNT), body mass index (BMI), waist-hip ratio (WHR), total cholesterol (TC), triglyceride (TG), high-density lipoproteins (HDL), low-density lipoproteins (LDL), homeostasis model assessment 2 for insulin resistance (HOMA2-IR), type 2 diabetes (T2D), ischemic heart disease (IHD), confidence interval (CI) and myocardial infarction (MI) are the abbreviations used in Table 1. The p values for significant difference are indicated in bold. Uncorrected p-values are shown, p-values significant after Bonferroni correction for multiple testing (p < 0.003) are indicated in bold. See also Tables S1–S10.
[a]Effective sample size calculated in DIAGRAM.

Male *Tm6sf2* KI mice exhibited higher glucose levels on a chow diet

To explore the mechanistic aspects underlying the complex biology at this locus, we generated *Tm6sf2* E167K knock-in (*Tm6sf2* KI) mice (C57BL/6J background) using CRISPR/Cas9 technology. The variant knock-in was validated by DNA sequencing (Figure S1A). The expression of *Tm6sf2* at the mRNA level was not changed in the *Tm6sf2* KI mice when compared with the wild-type (Wt) mice (Figure S1B). *Tm6sf2* KI had no significant effect on lipid accumulation in the liver, assessed by H&E staining and Oil Red O staining of liver sections from male mice on a chow diet (Figures S2A and S2B). We also measured the effects of the *Tm6sf2* KI variant on the plasma lipid profile. The male *Tm6sf2* KI mice displayed reduced plasma TC and TGs (Figure S2C). To evaluate whether the coding variant affects insulin sensitivity and glucose tolerance *in vivo*, we performed insulin tolerance test (ITT) and oral glucose tolerance test (OGTT) in the male *Tm6sf2* KI mice and Wt mice (Figures S2D and S2E). On chow diet, the male *Tm6sf2* KI mice exhibited significantly higher glucose levels, as shown by increased blood glucose level at the time point of 15 min and the corresponding area under the curve (AUC) during OGTT (Figure S2D). However, the incremental AUC shows no significant difference between the two groups. Although *Tm6sf2* KI increased glucose levels during ITT at the time points of 60 and 90 min and the corresponding AUC, there was no significant difference in the incremental AUC (Figure S2E). When blood glucose levels were expressed as a percentage of the baseline, the AUC has no significant difference between the two groups (Figure S2F). These findings suggest that the *Tm6sf2* E167K variant has modest effects on glucose and insulin tolerance in male mice fed a standard chow diet.

Aggravated glucose intolerance in male *Tm6sf2* KI mice on a high-fat diet

Next, we evaluated the effects of the E167 variant on hepatic steatosis, lipid, and glucose metabolism during a high-fat diet (HFD) challenge. H&E and Oil Red O staining revealed a significant increase in hepatic steatosis in male *Tm6sf2* KI mice (Figures 2A and 2B). Furthermore, male *Tm6sf2* KI mice showed a significant decrease in plasma TG without significant differences in TC, HDL-C, and LDL-C (Figure S3). Starting from week 11 on HFD, the male *Tm6sf2* KI mice showed increased fasting glucose (fasted 16 h) compared
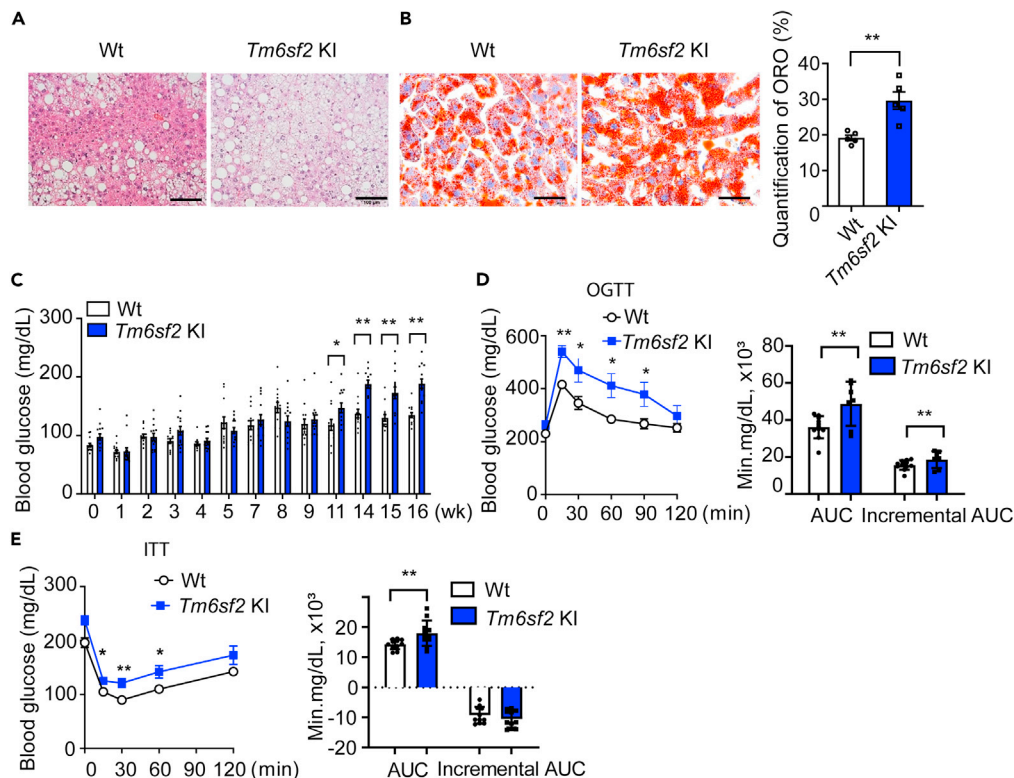
Figure 2. Impaired glucose tolerance in the male *Tm6sf2* KI mice fed a high-fat diet (HFD)
Tm6sf2 KI mice and Wt male mice were fed an HFD.
(A) H&E staining of the liver. Scale bar represents 100 μm.
(B) Oil red O (ORO) staining for the liver and corresponding quantification (n = 5/group). Scale bar represents 50 μm.
(C) The fasting glucose levels (fasted 16 h) were higher in male *Tm6sf2* KI mice compared with male Wt mice at the indicated time points after HFD feeding (n = 13-14/group).
(D and E) Higher glucose levels in male *Tm6sf2* KI mice compared with male Wt mice assessed by (D) OGTT (n = 7-11/group) and (E) ITT (n = 11/group), with the corresponding AUC (area under the curve) and incremental AUC plots in (D and E) on the right side. Values are mean ± SEM, *p < 0.05, **p < 0.01. Analysis in (B) used unpaired two-tailed t-test. Analysis in (C) and the left images of (D) and (E) used two-way analysis of variance (ANOVA) with Bonferroni correction and those for AUC in (D) and (E) used unpaired two-tailed t-test.
See also Figures S3 and S4.

with male Wt mice (Figure 2C). Notably, after 18 weeks on HFD, the male *Tm6sf2* KI mice displayed significantly aggravated glucose intolerance evidenced by increased blood glucose levels at the time points of 15, 30, 60, and 90 min during OGTT as well as by an increased AUC and incremental AUC compared to Wt mice (Figure 2D). *Tm6sf2* E167K KI also increased blood glucose levels at the time points of 15, 30, and 60 min and corresponding AUC during ITT (Figure 2E). However, the incremental AUC shows no significant difference between the two groups. Similarly, when blood glucose levels were expressed as a percentage of the baseline, there is no significant difference in insulin sensitivity between the *Tm6sf2* KI mice and Wt mice (Figure S4). Our data suggest that the *Tm6sf2* coding variant induces both hepatic steatosis and glucose intolerance in the male mice on HFD.

Female *Tm6sf2* KI mice do not exhibit glucose intolerance either on chow diet or on HFD

To determine whether the coding variant affects hepatic steatosis and glucose tolerance in a sex-specific fashion *in vivo*, we measured hepatic lipid accumulation and blood glucose levels in the female *Tm6sf2* KI mice. H&E staining and Oil Red O staining showed that *Tm6sf2* KI had no significant effect on lipid accumulation in the liver of female mice on chow diet (Figures S5A and S5B). Female *Tm6sf2* KI mice only showed decreased plasma TG (Figure S5C). No significant difference in glucose tolerance was observed in the female *Tm6sf2* KI mice on chow diet (Figures S5D and S5E).
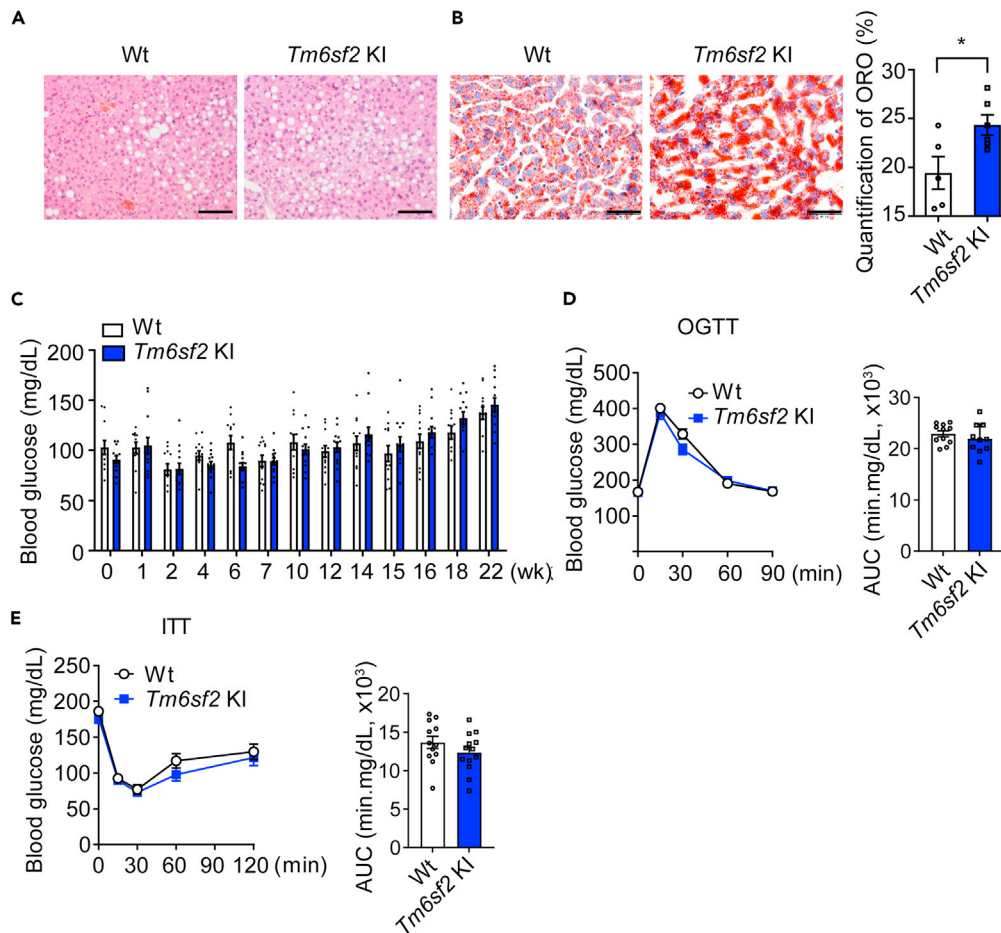
Figure 3. No changes in glucose tolerance in female *Tm6sf2* KI mice were fed an HFD

Tm6sf2 KI mice and Wt female mice were fed an HFD.

(A) H&E staining of the liver. Scale bar represents 100 μm.

(B) ORO staining for the liver and corresponding quantification (n = 5-6/group). Scale bar represents 50 μm.

(C) The fasting glucose levels (fasted 16 h) were not significantly different in female *Tm6sf2* KI mice at the indicated time points after HFD feeding (n = 12-13/group).

(D and E) No significant differences in glucose levels were observed in the female *Tm6sf2* KI mice assessed by (D) OGTT (n = 11/group) and (E) ITT (n = 12-13/group), with the corresponding AUC and incremental AUC plots in (D) and (E) on the right side. Values are mean ± SEM, *p < 0.05. Analysis in (B) used unpaired two-tailed t-test. Analysis in (C) and the left images of (D) and (E) used two-way ANOVA with Bonferroni correction and those for AUC in (D) and (E) used unpaired two-tailed t-test.

See also Figure S6.

On HFD, female *Tm6sf2* KI mice showed increased hepatic steatosis (Figures 3A and 3B) and decreased plasma TG (Figure S6) as found in male *Tm6sf2* KI mice. However, unlike the male *Tm6sf2* KI mice, no significant differences in fasting blood glucose (Figure 3C) were observed in the female *Tm6sf2* KI mice when compared with Wt mice, even after extended HFD feeding (22 weeks). Moreover, no significant differences in OGTT and ITT were found in the female *Tm6sf2* KI mice (Figures 3D and 3E). Insulin is crucial to maintain glucose homeostasis *in vivo*. We measured the plasma insulin level in the male and female *Tm6sf2* KI mice fasted 16 h. There was no significant difference in plasma insulin in the male or female *Tm6sf2* KI mice fed either a chow diet or an HFD when compared with the Wt mice (Figure S7). Taken together, our data indicate that the *Tm6sf2* E167K variant did not significantly affect glucose tolerance in females.
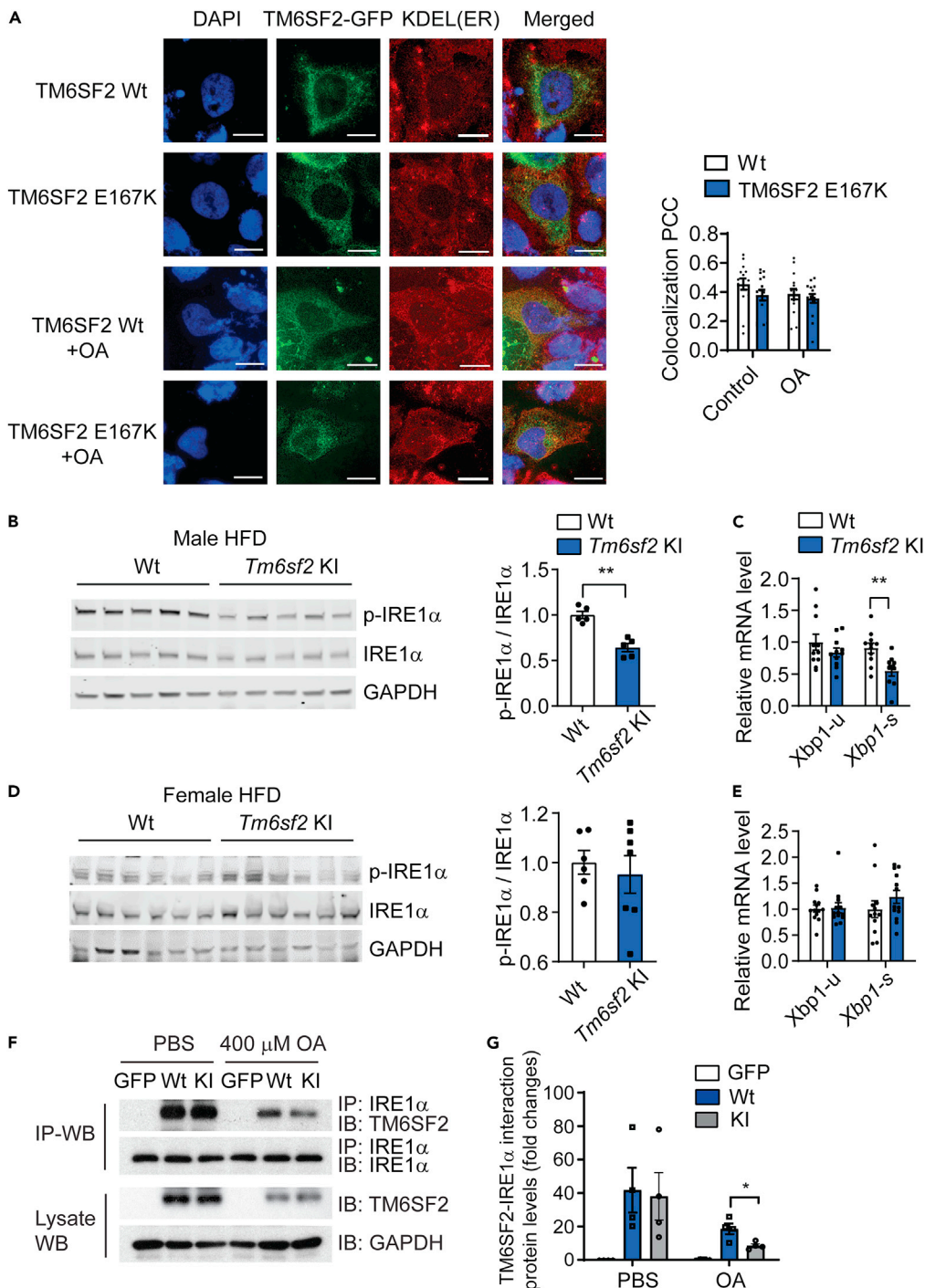
Figure 4. Impaired IRE1α-XBP1 signaling in male *Tm6sf2* KI mice were fed an HFD

(A) TM6SF2 subcellular localization was measured by immunofluorescence of TM6SF2 fused with GFP protein (TM6SF2-GFP) and TM6SF2-GFP containing E167K variant. After transfection of TM6SF2 expression vector, Huh-7 cells were treated with ethanol (control) or oleic acid (OA, 400 μM) for 18 h. Colocalization was quantified by Pearson's correlation coefficient (PCC). KDEL, an ER C-terminal tetrapeptide retention signal (Lys-Asp-Glu-Leu), was used an ER marker. Scale bar represents 20 μm.

(B and C) The male *Tm6sf2* KI mice and (D and E) female *Tm6sf2* KI mice were fed an HFD. (B) and (D) Total and phosphorylated IRE1α in the liver was determined by western blot (n = 5/group). The band intensity of phosphorylated IRE1α was analyzed quantitatively and normalized to total IRE1α. (C) and (E) Unspliced X-box-binding protein 1 (XBP1u)

Figure 4. *Continued*
and spliced Xbp1 (Xbp1-s) were determined by quantitative PCR (C, n = 9-11/group for male and E, n = 12-13/group for female). Values are mean ± SEM, *p < 0.05, **p < 0.01. Analysis in (B–E) used unpaired two-tailed t-test. (F and G) TM6SF2 interacted with IRE1α and E167K mutant attenuated the interaction in Huh-7 cells in the presence of oleic acid (OA) (F). The input of IRE1α protein for immunoprecipitation (IP)-western blot (WB) and the levels of GAPDH were determined as input controls (lysate WB). The pulled-down TM6SF2 was quantitatively analyzed in (G). Values are mean ± SD, *p < 0.05. Analysis in (G) used two-way ANOVA with Bonferroni correction.
See also Figure S8.

Impaired ER to nucleus signaling 1 (IRE1α) – X-box binding protein 1 (XBP1) signaling in male *Tm6sf2*KI mice on HFD

TM6SF2 is a transmembrane protein localized at the ER membrane (Mahdessian et al., 2014), whereby it reduces VLDL and ApoB secretion (Smagris et al., 2016). Consistent with previous results (Mahdessian et al., 2014), TM6SF2 is localized at the ER membrane measured by immunostaining in Huh-7 cells, a human hepatocyte established from male hepatoma tissue. However, the E167K variant did not alter the cellular localization of TM6SF2 (Figure 4A). High oleic acid (OA) can induce lipid overload in hepatocytes. OA treatment did not change the localization of either TM6SF2 or TM6SF2 E167K (Figure 4A). IRE1α, an ER-resident protein kinase and endoribonuclease, mediates the primary branch of the unfolded protein response (UPR) through splicing and enabling the mRNA encoding XBP1, a potent transcription factor (Hetz et al., 2020). The UPR signaling mediated through the IRE1α-XBP1 branch is critical to regulate hepatic lipid metabolism and insulin signaling (Herrema et al., 2016; Shao et al., 2014; Wang et al., 2018; Zhou et al., 2011). Although no significant changes in mRNA levels of ER stress-related genes were observed in male and female *Tm6sf2* KI mice on chow diet (Figures S8A and S8B), our data indicate that the levels of *Ire1α* mRNA (Figure S8C) and phosphorylated IRE1α protein (Figure 4B), the activated form of IRE1α, were decreased in the liver from male *Tm6sf2* KI mice on HFD. XBP1 is not only a critical component of the UPR but also an important transcription factor to facilitate energy metabolism (Herrema et al., 2016; Shao et al., 2014; Wang et al., 2018; Zhou et al., 2011). Upon ER stress, XBP1 is spliced by IRE1α to generate functional spliced XBP1 (XBP1s). We found that *Xbp1s* was suppressed in the liver from *Tm6sf2* KI male mice (Figure 4C). There were no differences in *Ire1α* mRNA, IRE1α phosphorylation, and *Xbp1* splicing between the two genotypes in the females (Figures 4D, 4E, and S8D).

Both IRE1α and TM6SF2 are ER membrane proteins. To determine whether IRE1α directly interacts with TM6SF2, we performed co-immunoprecipitation assays in Huh-7 cells in the absence or presence of OA. We found that IRE1α interacts with TM6SF2 in Huh-7 cells, and this interaction was reduced by the TM6SF2 E167K mutation under lipid overload conditions (Figures 4F and 4G), indicating a central role for this variant in TM6SF2-dependent regulation of glucose and lipid metabolism.

Gene expression analysis in the liver of *Tm6sf2*KI mice

The E167K variant perturbs IRE1α-XBP1 signaling and leads to hepatic steatosis and glucose intolerance in male mice, in which transcriptome changes can be involved. To identify the altered genes induced by the E167K variant, we performed a microarray analysis on liver samples from the *Tm6sf2* KI and Wt male mice on HFD (Figure 5A). Through analysis of the genes with altered expression in the liver of male *Tm6sf2* KI mice, we found glucose metabolism-related genes and further validated the microarray results by quantitative PCR (Figure 5B). Among these genes, two key metabolic genes, *Lpin 1* and *Ide*, were dysregulated in the liver of male *Tm6sf2* KI mice on HFD. LIPIN 1, an enzyme promoting TG biosynthesis and concurrently contributing to insulin resistance (Reue and Wang, 2019; Ryu et al., 2009), was upregulated, whereas insulin-degrading enzyme (IDE), an enzyme suppressing insulin resistance (Pivovarova et al., 2016; Villa-Perez et al., 2018), was downregulated at both the mRNA and protein levels in the liver of male *Tm6sf2* KI mice fed an HFD (Figures 5B and 5C). The expression of other glucose metabolism-related genes including nicotinamide nucleotide transhydrogenase (NNT) and ubiquitin-specific protease 2 (USP2) were also increased in the liver of male *Tm6sf2* KI mice. However, except for NNT which was also upregulated, the expression of IDE, LIPIN 1, and USP2 was not significantly changed in the liver of female *Tm6sf2* KI mice on HFD (Figures 5D and 5E).

Impaired AKT serine/threonine kinase 1 signaling in male *Tm6sf2*KI mice fed an HFD

AKT and glycogen synthase kinase 3 beta (GSK3β) are critical mediators for the intracellular signaling of insulin (Manning and Toker, 2017). In the liver of *Tm6sf2* KI male mice fed an HFD, the phosphorylation
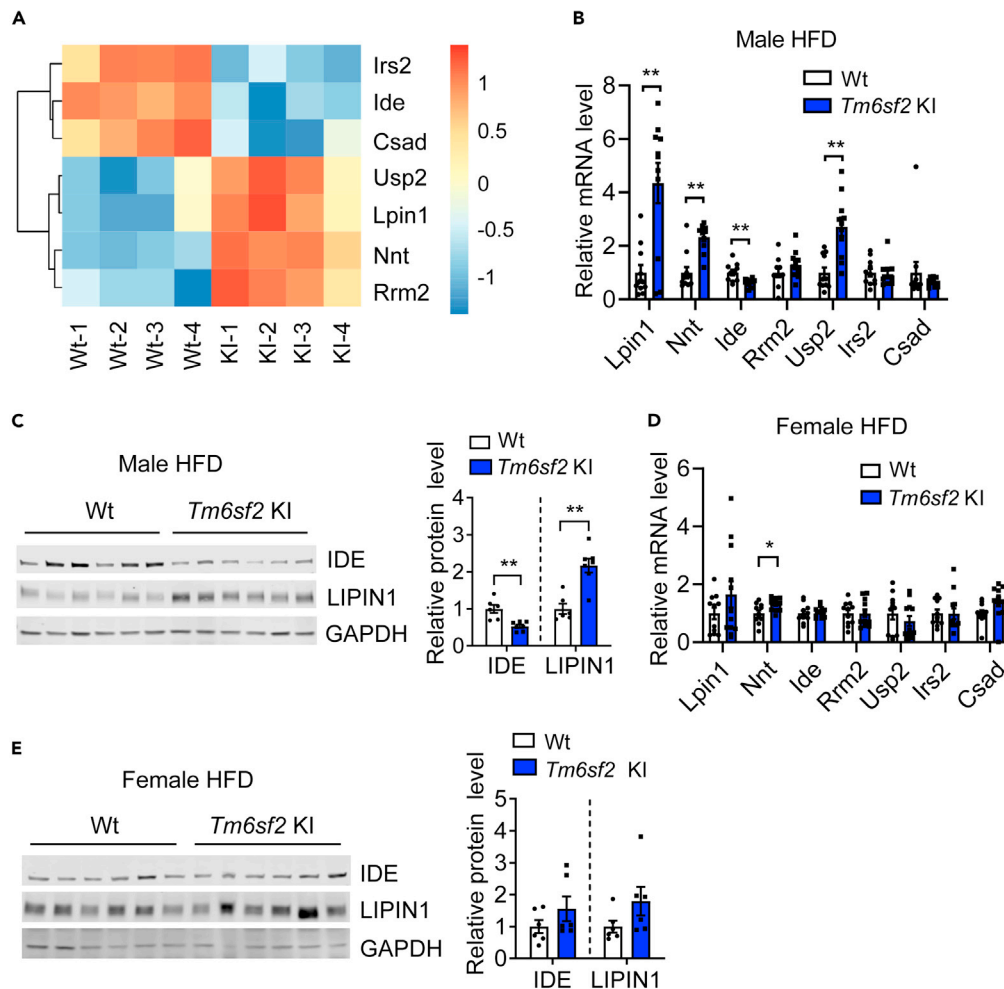
Figure 5. Transcriptome analysis in the liver of male *Tm6sf2* KI mice on HFD

(A) Transcriptomic analysis of gene expression in the liver of male *Tm6sf2* KI mice on HFD for 20 weeks (n = 4/group). Glucose metabolism-related genes are shown in heatmap.

(B) The expression of genes shown in (A) were determined by quantitative PCR (n = 11/group).

(C) The expression of IDE and LIPIN 1 in the liver of male *Tm6sf2* KI mice fed an HFD was significantly changed as determined by western blot and quantitatively analyzed (n = 6/group).

(D) Glucose metabolism-related genes were determined by quantitative PCR (n = 11/group) in the liver of female *Tm6sf2* KI mice on HFD for 22 weeks.

(E) The expression of IDE and LIPIN 1 in the liver of female mice fed an HFD was not significantly changed as determined by western blot (n = 6/group).

The band intensity in (C) and (E) was analyzed quantitatively and normalized to glyceraldehyde-3-phosphate dehydrogenase (GAPDH). Values are mean $\pm$ SEM, *p < 0.05, **p < 0.01. Analysis in (B–E) used unpaired two-tailed Student's t-test.

of AKT at Ser473 and the phosphorylation of GSK3β at Ser9 were significantly attenuated after insulin administration (Figures 6A and 6B), indicating increased hepatic insulin resistance. Unlike the male *Tm6sf2* KI mice, female *Tm6sf2* KI mice on HFD showed no change in the phosphorylation of AKT and GSK3β (Figures 6C and 6D). Our data indicate impaired insulin signaling in the liver of male *Tm6sf2* KI mice.

DISCUSSION

In the present study, we investigated the causal role of the *TM6SF2* rs58542926C >T variant in the development of glucose intolerance and the underlying mechanisms using a newly generated mouse model. Our data revealed that the variant leads to the development of hepatic steatosis and altered sex-specific
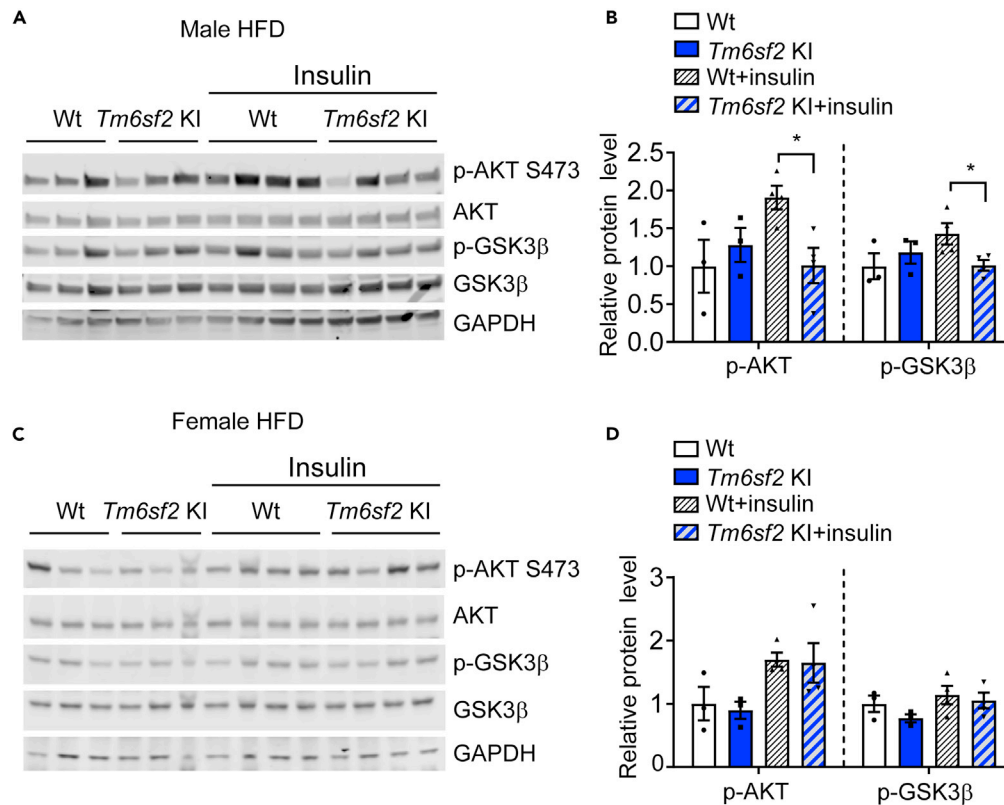
Figure 6. Attenuated AKT signaling in the male *Tm6sf2* KI mice fed an HFD

(A and B) Male *Tm6sf2* KI mice and (C and D) female *Tm6sf2* KI mice and their Wt counterpart mice were fed an HFD for 20 weeks. The phosphorylation of AKT and GSK3β was decreased in the liver of male *Tm6sf2* KI mice, whereas there were no significant differences in AKT and GSK3β phosphorylation in female *Tm6sf2* KI mice administered insulin. The total and phosphorylated AKT and GSK3β were determined by (A and C) western blot (n = 3-4/group). The band intensity of phosphorylated AKT and GSK3β was analyzed quantitatively and normalized to total AKT or GSK3β, respectively (B and D). Values are mean ± SEM, *p < 0.05. Analysis in (B) and (D) used two-way ANOVA with Bonferroni correction.

glucose metabolism. Mouse and human TM6SF2 proteins are approximately 78% identical, and E167 is conserved in humans and mice. Consistent with the findings observed in human *TM6SF2* E167K variant carriers, *Tm6sf2* E167K mice showed glucose intolerance and hepatic steatosis after HFD feeding, primarily in males. Interestingly, *Tm6sf2* KI causes glucose intolerance in male mice but not in female mice. This phenotype exhibiting sex-specific effects on glucose tolerance is consistent with our genetic analyses in human populations. Additional molecular analysis revealed important mechanisms underlying this phenotype.

In addition to environmental factors, common genetic variation in the form of single nucleotide polymorphisms may predispose individuals to T2D (Hirschhorn, 2009; Klein et al., 2010; Meyre, 2017). Our human genetic studies revealed that the *TM6SF2* coding variant is associated with an increased risk of T2D, blood glucose, and Hb1Ac, especially in males. The role of sex is a fundamental component in the incidence and evolution of diabetes (Kautzky-Willer et al., 2016; Mauvais-Jarvis, 2015). Multiple lines of evidence indicate that the T allele at the rs58542926 variant is associated with an increased risk of T2D (Kim et al., 2017; Liu et al., 2017; Musso et al., 2017). Here, we used knock-in mice of the T allele to study the sex-related association of rs58542926 with T2D and the functional role of TM6SF2 in glucose metabolism. We monitored the blood glucose changes in *Tm6sf2* KI mice under normal chow and HFD. Since *TM6SF2* is highly expressed in the liver (Fan et al., 2016; Holmen et al., 2014; Kozlitina et al., 2014; Mahdessian et al., 2014), we focused on the molecular alterations in the liver, which contribute to the regulation of lipid and glucose metabolism. The potential effects of the *Tm6sf2* coding variant on other metabolically active tissues such as skeletal muscle, adipose tissue, and small intestine warrant further investigation.

Both TM6SF2 and IRE1α are ER transmembrane proteins. IRE1α-XBP1 is one of the major UPR signaling pathways that have diverse effects on cellular processes (Lindholm et al., 2017; Salvado et al., 2015). *Ire1α* deficiency induces inflammatory responses and hepatic steatosis in mice (Wang et al., 2018). Xbp1s acts as a marker and downstream effector of IRE1α (Piperi et al., 2016). XBP1s reduces lipogenic gene expression and attenuates insulin resistance in mice (Herrema et al., 2016; Zhou et al., 2011). Increased TG accumulation and insulin resistance were found in the liver from *Xbp1s*-deficient mice (Shao et al., 2014). Thus, inhibition of IRE1α-XBP1s could act as a molecular mechanism underlying the *Tm6sf2* KI-induced hepatic steatosis and insulin resistance. We further found that, as an ER membrane protein, TM6SF2 interacts with IRE1α and that interaction was attenuated by the E167K coding variant (Figure 6E), suggesting that E167 is critical to maintain the physical interaction between TM6SF2 and IRE1α in the ER and that E167K leads to inhibition of IRE1α-XBP1 signaling.

Since TM6SF2 is an ER membrane protein, it cannot directly regulate gene expression. The E167K-dependent transcriptomic changes can be regulated by attenuated IRE1α-XBP1 signaling, be secondary to hepatic steatosis, or be genetic compensation. Our transcriptome analysis revealed potential genes that contribute to glucose intolerance in the *Tm6sf2* KI mice. LIPIN 1 is a critical enzyme that promotes TG biosynthesis. It is highly expressed in the liver and adipose tissue and catalyzes the conversion of phosphatidic acid into diacylglycerol (DAG) (Reue and Dwyer, 2009). LIPIN 1 overexpression increases the TG accumulation in the liver and adipose tissue, whereas *Lpin 1*-deficient mice show attenuated insulin resistance and TG accumulation after HFD feeding (Pivovarova et al., 2016; Villa-Perez et al., 2018). Another critical gene responsive to the *Tm6sf2* coding variant is *Ide*. IDE is highly expressed in the brain, liver, and pancreas (Pivovarova et al., 2016). Severe accumulation of amyloid β-protein (Aβ) in the brain is a feature of Alzheimer disease (AD) (Ohyagi et al., 2019). IDE is a potential candidate enzyme responsible for the degradation and clearance of Aβ. Liver-specific *Ide*-deficient mice showed glucose intolerance and impaired AKT signaling (Villa-Perez et al., 2018). In our study, blood insulin levels were not significantly changed in either male or female *Tm6sf2* KI mice. However, AKT signaling was significantly attenuated in the liver of male *Tm6sf2* KI mice. The upregulated LIPIN 1 and downregulated IDE could lead to the decreased AKT signaling in the liver of male *Tm6sf2* KI mice.

Our data suggest that in addition to upregulated *Lpin 1* and downregulated *Ide*, other glucose metabolism-related genes including NNT and USP2 were also altered in the liver of male *Tm6sf2* KI mice. NNT activity is positively correlated with increased susceptibility to severe diabetes after becoming obese in mice (Aston-Mourney et al., 2007). USP2 increases hepatic gluconeogenesis and exacerbates glucose intolerance in diet-induced obese mice (Molusky et al., 2012). Thus, these dysregulated glucose metabolism-related genes in the liver could at least partially account for the hepatic insulin resistance caused by *Tm6sf2* KI.

In conclusion, we provide evidence that the *TM6SF2* E167K variant is associated with T2D, specifically in male humans and mice. *Tm6sf2* E167K KI causes impaired glucose tolerance in male mice. We uncovered molecular mechanisms underlying the *Tm6sf2* KI-dependent glucose disorders in mice. Our results have relevance for the treatment of T2D and would lead to a deep understanding of the TM6SF2 coding variant, a potential target for precise treatment of fatty liver diseases and T2D.

Limitations of the study

It should be noted that the challenge of HFD is commonly used to induce glucose intolerance and insulin resistance in mouse models (Winzell and Ahrén, 2004). High-fat high-sucrose diet challenge can rapidly induce metabolic alterations, including obesity, glucose intolerance, insulin resistance, and liver lipid accumulation in mice (Burchfield et al., 2018; Yang et al., 2012), serving as an alternative mouse model for metabolic syndrome. The effects of rs58542926C >T variant on glucose metabolism and fatty liver diseases in this model deserve future studies. The effect of *Tm6sf2* coding variant on nonalcoholic steatohepatitis and cirrhosis will be determined in follow-up studies using appropriate animal models and diets (Friedman et al., 2018; Rom et al., 2019, 2020). In this study, we cannot exclude that the plasma insulin may be relatively higher in female mice compared to males during OGTT. The potential effects of *Tm6sf2* coding variant on insulin secretion and pancreatic β-cell function after HFD feeding warrant further investigation. In addition, whether sex steroid hormones such as estrogen, progesterone, and androgen mediate the sex-specific effect of *Tm6sf2* KI on glucose metabolism will be explored in future studies.

STAR★METHODS

Detailed methods are provided in the online version of this paper and include the following:

- KEY RESOURCES TABLE
- RESOURCE AVAILABILITY
  - Lead contact
  - Materials availability
  - Data and code availability
- EXPERIMENTAL MODEL AND SUBJECT DETAILS
  - Animals
  - Cell lines and primary cultures
  - Binary trait genetic association studies
  - Quantitative trait genetic association studies
  - The Nord-Trøndelag Health Study (HUNT)
  - Statistical analysis of genetic association studies
- METHOD DETAILS
  - Glucose tolerance test and insulin tolerance test
  - Liver samples, plasma insulin measurement and Lipid Profiles
  - Quantitative PCR
  - Western blot
  - Immunofluorescence
  - Cell culture and oleic acid (OA) treatment
  - Co-immunoprecipitation (Co-IP) analysis
  - Histology
  - Microarray analysis
- QUANTIFICATION AND STATISTICAL ANALYSIS

SUPPLEMENTAL INFORMATION

Supplemental information can be found online at https://doi.org/10.1016/j.isci.2021.103196.

AUTHOR CONTRIBUTIONS

Y.F., B.N.W., H.L., J.S., W.L., W.Z., K.Z., and H.K. obtained, contributed, and analyzed the phenotype data. B.N.W. was responsible for sample selection. B.N.W. and W.Z. were responsible for genetic data analysis and interpretation with assistance from S.E.G., I.S., S.R., L.F., J.B.N., M.E.G., and K.H. Y.F., B.N.W., and W.Z. generated figures and performed secondary analyses. A.M. was responsible for replication in DIAGRAM Consortium. Y.F., H.L., J.S., W.L., and Z.L. conducted transcriptomic analysis mouse experiments with assistance from O.R., D.Y., J.S., and J.Z. Y.F. drafted the manuscript with assistance from B.N.W. Y.E.C., J.Z., O.R., W.L., K.Z., M.T.G., and C.J.W. critically reviewed the manuscript and provided comments and feedback. Y.F. and Y.E.C. conceived the study. Y.F., C.J.W., and Y.E.C. designed the study. Y.F., C.J.W., and Y.E.C. provided overall leadership for the project.

DECLARATION OF INTERESTS

As of June 2020, A.M. is an employee of Genentech and a holder of Roche stock. The spouse of C.J.W. works at Regeneron Pharmaceuticals. J.B.N. works at Regeneron Pharmaceuticals.

REFERENCES

Aston-Mourney, K., Wong, N., Kebede, M., Zraika, S., Balmer, L., McMahon, J.M., Fam, B.C., Favaloro, J., Proietto, J., Morahan, G., and Andrikopoulos, S. (2007). Increased nicotinamide nucleotide transhydrogenase levels predispose to insulin hypersecretion in a mouse strain susceptible to diabetes. Diabetologia 50, 2476–2485. https://doi.org/10.1007/s00125-007-0814-x.

Bethel, M.A., Stevens, S.R., Buse, J.B., Choi, J., Gustavson, S.M., Iqbal, N., Lokhnygina, Y., Mentz, R.J., Patel, R.A., Ohman, P., et al. (2020). Exploring the possible impact of unbalanced open-label drop-in of glucose-lowering medications on EXSCEL outcomes. Circulation. https://doi.org/10.1161/CIRCULATIONAHA.119.043353.

Burchfield, J.G., Kebede, M.A., Meoli, C.C., Stockli, J., Whitworth, P.T., Wright, A.L., Hoffman, N.J., Minard, A.Y., Ma, X., Krycer, J.R., et al. (2018). High dietary fat and sucrose results in an extensive and time-dependent deterioration in health of multiple physiological systems in mice. J. Biol. Chem. 293, 5731–5745. https://doi.org/10.1074/jbc.RA117.000808.

Bycroft, C., Freeman, C., Petkova, D., Band, G., Elliott, L.T., Sharp, K., Motyer, A., Vukcevic, D., Delaneau, O., O'Connell, J., et al. (2018). The UK Biobank resource with deep phenotyping and genomic data. Nature 562, 203–209. https://doi.org/10.1038/s41586-018-0579-z.

Dongiovanni, P., Petta, S., Maglio, C., Fracanzani, A.L., Pipitone, R., Mozzi, E., Motta, B.M., Kaminska, D., Rametta, R., Grimaudo, S., et al. (2015). Transmembrane 6 superfamily member 2 gene variant disentangles nonalcoholic steatohepatitis from cardiovascular disease. Hepatology 61, 506–514. https://doi.org/10.1002/hep.27490.

Dupuis, J., Langenberg, C., Prokopenko, I., Saxena, R., Soranzo, N., Jackson, A.U., Wheeler, E., Glazer, N.L., Bouatia-Naji, N., Gloyn, A.L., et al. (2010). New genetic loci implicated in fasting glucose homeostasis and their impact on type 2 diabetes risk. Nat. Genet. 42, 105–116. https://doi.org/10.1038/ng.520.

Fan, Y., Lu, H., Guo, Y., Zhu, T., Garcia-Barrio, M.T., Jiang, Z., Willer, C.J., Zhang, J., and Chen, Y.E. (2016). Hepatic transmembrane 6 superfamily member 2 regulates cholesterol metabolism in mice. Gastroenterology 150, 1208–1218. https://doi.org/10.1053/j.gastro.2016.01.005.

Firneisz, G. (2014). Non-alcoholic fatty liver disease and type 2 diabetes mellitus: the liver disease of our age? World J. Gastroenterol. 20, 9072–9089. https://doi.org/10.3748/wjg.v20.i27.9072.

Friedman, S.L., Neuschwander-Tetri, B.A., Rinella, M., and Sanyal, A.J. (2018). Mechanisms of NAFLD development and therapeutic strategies. Nat. Med. 24, 908–922. https://doi.org/10.1038/s41591-018-0104-9.

Herrema, H., Zhou, Y., Zhang, D., Lee, J., Salazar Hernandez, M.A., Shulman, G.I., and Ozcan, U. (2016). XBP1s is an anti-lipogenic protein. J. Biol. Chem. 291, 17394–17404. https://doi.org/10.1074/jbc.M116.728949.

Hetz, C., Zhang, K., and Kaufman, R.J. (2020). Mechanisms, regulation and functions of the unfolded protein response. Nat. Rev. Mol.Cell Biol. 21, 421–438. https://doi.org/10.1038/s41580-020-0250-z.

Hirschhorn, J.N. (2009). Genomewide association studies–illuminating biologic pathways. N. Engl. J. Med. 360, 1699–1701. https://doi.org/10.1056/NEJMp0808934.

Holmen, O.L., Zhang, H., Fan, Y., Hovelson, D.H., Schmidt, E.M., Zhou, W., Guo, Y., Zhang, J., Langhammer, A., Lochen, M.L., et al. (2014). Systematic evaluation of coding variation identifies a candidate causal variant in TM6SF2 influencing total cholesterol and myocardial infarction risk. Nat. Genet. 46, 345–351. https://doi.org/10.1038/ng.2926.

Kahali, B., Liu, Y.L., Daly, A.K., Day, C.P., Anstee, Q.M., and Speliotes, E.K. (2015). TM6SF2: catch-22 in the fight against nonalcoholic fatty liver disease and cardiovascular disease? Gastroenterology 148, 679–684. https://doi.org/10.1053/j.gastro.2015.01.038.

Kautzky-Willer, A., Harreiter, J., and Pacini, G. (2016). Sex and gender differences in risk, pathophysiology and complications of type 2 diabetes mellitus. Endocr. Rev. 37, 278–316. https://doi.org/10.1210/er.2015-1137.

Kim, D.S., Jackson, A.U., Li, Y.K., Stringham, H.M., FinMetSeq, I., Kuusisto, J., Kangas, A.J., Soininen, P., Ala-Korpela, M., Burant, C.F., et al. (2017). Novel association of TM6SF2 rs58542926 genotype with increased serum tyrosine levels and decreased apoB-100 particles in Finns. J. Lipid Res. 58, 1471–1481. https://doi.org/10.1194/jlr.P076034.

Klein, R.J., Xu, X., Mukherjee, S., Willis, J., and Hayes, J. (2010). Successes of genome-wide association studies. Cell 142, 350–351. author reply 353-355. https://doi.org/10.1016/j.cell.2010.07.026.

Kozlitina, J., Smagris, E., Stender, S., Nordestgaard, B.G., Zhou, H.H., Tybjaerg-Hansen, A., Vogt, T.F., Hobbs, H.H., and Cohen, J.C. (2014). Exome-wide association study identifies a TM6SF2 variant that confers susceptibility to nonalcoholic fatty liver disease. Nat. Genet. 46, 352–356. https://doi.org/10.1038/ng.2901.

Lang, P., Hasselwander, S., Li, H., and Xia, N. (2019). Effects of different diets used in diet-induced obesity models on insulin resistance and vascular dysfunction in C57BL/6 mice. Sci. Rep. 9, 19556.

Lindholm, D., Korhonen, L., Eriksson, O., and Koks, S. (2017). Recent insights into the role of unfolded protein response in ER stress in health and disease. Front.Cell Dev. Biol. 5, 48. https://doi.org/10.3389/fcell.2017.00048.

Liu, D.J., Peloso, G.M., Yu, H., Butterworth, A.S., Wang, X., Mahajan, A., Saleheen, D., Emdin, C., Alam, D., Alves, A.C., et al. (2017). Exome-wide association study of plasma lipids in >300,000 individuals. Nat. Genet. 49, 1758–1766. https://doi.org/10.1038/ng.3977.

Liu, Y.L., Reeves, H.L., Burt, A.D., Tiniakos, D., McPherson, S., Leathart, J.B., Allison, M.E., Alexander, G.J., Piguet, A.C., Anty, R., et al. (2014). TM6SF2 rs58542926 influences hepatic fibrosis progression in patients with non-alcoholic fatty liver disease. Nat. Commun. 5, 4309. https://doi.org/10.1038/ncomms5309.

Mahajan, A., Taliun, D., Thurner, M., Robertson, N.R., Torres, J.M., Rayner, N.W., Payne, A.J., Steinthorsdottir, V., Scott, R.A., Grarup, N., et al. (2018). Fine-mapping type 2 diabetes loci to single-variant resolution using high-density imputation and islet-specific epigenome maps. Nat. Genet. 50, 1505–1513. https://doi.org/10.1038/s41588-018-0241-6.

Mahdessian, H., Taxiarchis, A., Popov, S., Silveira, A., Franco-Cereceda, A., Hamsten, A., Eriksson, P., and van't Hooft, F. (2014). TM6SF2 is a regulator of liver fat metabolism influencing triglyceride secretion and hepatic lipid droplet content. Proc. Natl. Acad. Sci. U S A 111, 8913–8918. https://doi.org/10.1073/pnas.1323785111.

Mann, G.E., Yudilevich, D.L., and Sobrevia, L. (2003). Regulation of amino acid and glucose transporters in endothelial and smooth muscle cells. Physiol. Rev. 83, 183–252. https://doi.org/10.1152/physrev.00022.2002.

Manning, B.D., and Toker, A. (2017). AKT/PKB signaling: Navigating the network. Cell 169, 381–405. https://doi.org/10.1016/j.cell.2017.04.001.

Mauvais-Jarvis, F. (2015). Sex differences in metabolic homeostasis, diabetes, and obesity. Biol.SexDiffer. 6, 14. https://doi.org/10.1186/s13293-015-0033-y.

Meyre, D. (2017). Give GWAS a chance. Diabetes 66, 2741–2742. https://doi.org/10.2337/dbi17-0026.

Molusky, M.M., Li, S., Ma, D., Yu, L., and Lin, J.D. (2012). Ubiquitin-specific protease 2 regulates hepatic gluconeogenesis and diurnal glucose metabolism through 11β-hydroxysteroid dehydrogenase 1. Diabetes 61, 1025–1035. https://doi.org/10.2337/db11-0970.

Moravcova, A., Cervinkova, Z., Kucera, O., Mezera, V., Rychtrmoc, D., and Lotkova, H. (2015). The effect of oleic and palmitic acid on induction of steatosis and cytotoxicity on rat hepatocytes in

primary culture. Physiol. Res. 64 (Suppl 5), S627–S636.

Musso, G., Cipolla, U., Cassader, M., Pinach, S., Saba, F., De Michieli, F., Paschetta, E., Bongiovanni, D., Framarin, L., Leone, N., et al. (2017). TM6SF2 rs58542926 variant affects postprandial lipoprotein metabolism and glucose homeostasis in NAFLD. J. Lipid Res. 58, 1221–1229. https://doi.org/10.1194/jlr.M075028.

O'Hare, E.A., Yang, R., Yerges-Armstrong, L.M., Sreenivasan, U., McFarland, R., Leitch, C.C., Wilson, M.H., Narina, S., Gorden, A., Ryan, K.A., et al. (2017). TM6SF2 rs58542926 impacts lipid processing in liver and small intestine. Hepatology 65, 1526–1542. https://doi.org/10.1002/hep.29021.

Ohyagi, Y., Miyoshi, K., and Nakamura, N. (2019). Therapeutic strategies for Alzheimer's disease in the view of diabetes mellitus. Adv. Exp. Med. Biol. 1128, 227–248. https://doi.org/10.1007/978-981-13-3540-2_11.

Piperi, C., Adamopoulos, C., and Papavassiliou, A.G. (2016). XBP1: a pivotal transcriptional regulator of glucose and lipid metabolism. Trends Endocrinol.Metab. 27, 119–122. https://doi.org/10.1016/j.tem.2016.01.001.

Pivovarova, O., Hohn, A., Grune, T., Pfeiffer, A.F., and Rudovich, N. (2016). Insulin-degrading enzyme: new therapeutic target for diabetes and Alzheimer's disease? Ann. Med. 48, 614–624. https://doi.org/10.1080/07853890.2016.1197416.

Pulit, S.L., Stoneman, C., Morris, A.P., Wood, A.R., Glastonbury, C.A., Tyrrell, J., Yengo, L., Ferreira, T., Marouli, E., Ji, Y., et al. (2019). Meta-analysis of genome-wide association studies for body fat distribution in 694 649 individuals of European ancestry. Hum. Mol. Genet. 28, 166–174. https://doi.org/10.1093/hmg/ddy327.

Reue, K., and Dwyer, J.R. (2009). Lipin proteins and metabolic homeostasis. J. Lipid Res. 50 (Suppl), S109–S114. https://doi.org/10.1194/jlr.R800052-JLR200.

Reue, K., and Wang, H. (2019). Mammalian lipin phosphatidic acid phosphatases in lipid synthesis and beyond: metabolic and inflammatory disorders. J. Lipid Res. 60, 728–733. https://doi.org/10.1194/jlr.S091769.

Rom, O., Liu, Y., Liu, Z., Zhao, Y., Wu, J., Ghrayeb, A., Villacorta, L., Fan, Y., Chang, L., Wang, L., et al. (2020). Glycine-based treatment ameliorates NAFLD by modulating fatty acid oxidation, glutathione synthesis, and the gut microbiome. Sci. Transl. Med. 12. https://doi.org/10.1126/scitranslmed.aaz2841.

Rom, O., Xu, G., Guo, Y., Zhu, Y., Wang, H., Zhang, J., Fan, Y., Liang, W., Lu, H., Liu, Y., et al. (2019). Nitro-fatty acids protect against steatosis and fibrosis during development of nonalcoholic fatty liver disease in mice. EBioMedicine 41, 62–72. https://doi.org/10.1016/j.ebiom.2019.02.019.

Ryu, D., Oh, K.J., Jo, H.Y., Hedrick, S., Kim, Y.N., Hwang, Y.J., Park, T.S., Han, J.S., Choi, C.S., Montminy, M., and Koo, S.H. (2009). TORC2 regulates hepatic insulin signaling via a mammalian phosphatidic acid phosphatase, LIPIN1. Cell Metab. 9, 240–251. https://doi.org/10.1016/j.cmet.2009.01.007.

Salvado, L., Palomer, X., Barroso, E., and Vazquez-Carrera, M. (2015). Targeting endoplasmic reticulum stress in insulin resistance. Trends Endocrinol.Metab. 26, 438–448. https://doi.org/10.1016/j.tem.2015.05.007.

Shao, M., Shan, B., Liu, Y., Deng, Y., Yan, C., Wu, Y., Mao, T., Qiu, Y., Zhou, Y., Jiang, S., et al. (2014). Hepatic IRE1alpha regulates fasting-induced metabolic adaptive programs through the XBP1s-PPARalpha axis signalling. Nat. Commun. 5, 3528. https://doi.org/10.1038/ncomms4528.

Smagris, E., Gilyard, S., BasuRay, S., Cohen, J.C., and Hobbs, H.H. (2016). Inactivation of Tm6sf2, a gene defective in fatty liver disease, impairs lipidation but not secretion of very low density lipoproteins. J. Biol. Chem. 291, 10659–10676. https://doi.org/10.1074/jbc.M116.719955.

Small, K.S., Todorcevic, M., Civelek, M., El-Sayed Moustafa, J.S., Wang, X., Simon, M.M., Fernandez-Tajes, J., Mahajan, A., Horikoshi, M., Hugill, A., et al. (2018). Regulatory variants at KLF14 influence type 2 diabetes risk via a female-specific effect on adipocyte size and body composition. Nat. Genet. 50, 572–580. https://doi.org/10.1038/s41588-018-0088-x.

Sookoian, S., Castano, G.O., Scian, R., Mallardi, P., Fernandez Gianotti, T., Burgueno, A.L., San Martino, J., and Pirola, C.J. (2015). Genetic variation in transmembrane 6 superfamily member 2 and the risk of nonalcoholic fatty liver disease and histological disease severity. Hepatology 61, 515–525. https://doi.org/10.1002/hep.27556.

Villa-Perez, P., Merino, B., Fernandez-Diaz, C.M., Cidad, P., Lobaton, C.D., Moreno, A., Muturi, H.T., Ghadieh, H.E., Najjar, S.M., Leissring, M.A., et al. (2018). Liver-specific ablation of insulin-degrading enzyme causes hepatic insulin resistance and glucose intolerance, without affecting insulin clearance in mice. Metabolism 88, 1–11. https://doi.org/10.1016/j.metabol.2018.08.001.

Wang, J.M., Qiu, Y., Yang, Z., Kim, H., Qian, Q., Sun, Q., Zhang, C., Yin, L., Fang, D., Back, S.H., et al. (2018). IRE1alpha prevents hepatic steatosis by processing and promoting the degradation of select microRNAs. Sci.Signal. 11. https://doi.org/10.1126/scisignal.aao4617.

Wei, W.Q., Bastarache, L.A., Carroll, R.J., Marlo, J.E., Osterman, T.J., Gamazon, E.R., Cox, N.J., Roden, D.M., and Denny, J.C. (2017). Evaluating phecodes, clinical classification software, and ICD-9-CM codes for phenome-wide association studies in the electronic health record. PLoS One 12, e0175508. https://doi.org/10.1371/journal.pone.0175508.

Willer, C.J., Li, Y., and Abecasis, G.R. (2010). METAL: fast and efficient meta-analysis of genomewide association scans. Bioinformatics 26, 2190–2191. https://doi.org/10.1093/bioinformatics/btq340.

Winkler, T.W., Justice, A.E., Cupples, L.A., Kronenberg, F., Kutalik, Z., Heid, I.M., and consortium, G. (2017). Approaches to detect genetic effects that differ between two strata in genome-wide meta-analyses: Recommendations based on a systematic evaluation. PLoS One 12, e0181038. https://doi.org/10.1371/journal.pone.0181038.

Winzell, M.S., and Ahrén, B. (2004). The high-fat diet–fed mouse.A model for studying mechanisms and treatment of impaired glucose tolerance and type 2 diabetes. Diabetes 53, S215–S219. https://doi.org/10.2337/diabetes.53.suppl_3.S215.

Yang, Z.H., Miyahara, H., Takeo, J., and Katayama, M. (2012). Diet high in fat and sucrose induces rapid onset of obesity-related metabolic syndrome partly through rapid response of genes involved in lipogenesis, insulin signalling and inflammation in mice. Diabetol.Metab.Syndr. 4, 32. https://doi.org/10.1186/1758-5996-4-32.

Zhou, W., Nielsen, J.B., Fritsche, L.G., Dey, R., Gabrielsen, M.E., Wolford, B.N., LeFaive, J., VandeHaar, P., Gagliano, S.A., Gifford, A., et al. (2018). Efficiently controlling for case-control imbalance and sample relatedness in large-scale genetic association studies. Nat. Genet. 50, 1335–1341. https://doi.org/10.1038/s41588-018-0184-y.

Zhou, Y., Lee, J., Reno, C.M., Sun, C., Park, S.W., Chung, J., Lee, J., Fisher, S.J., White, M.F., Biddinger, S.B., and Ozcan, U. (2011). Regulation of glucose homeostasis through a XBP-1-FoxO1 interaction. Nat. Med. 17, 356–365. https://doi.org/10.1038/nm.2293.

STAR★METHODS

KEY RESOURCES TABLE

REAGENT or RESOURCE	SOURCE	IDENTIFIER
Antibodies		
Lipin 1 (D2W9G) Rabbit mAb	Cell Signaling	#14906; RRID: AB_2798644
Akt (pan) (C67E7) Rabbit mAb	Cell Signaling	#4691; RRID: AB_915783
Phospho-Akt (Ser473) (D9E) Rabbit mAb	Cell Signaling	#4060; RRID: AB_2315049
GSK-3β (D5C5Z) Rabbit mAb	Cell Signaling	#12456; RRID: AB_2636978
Phospho-GSK-3β (Ser9) (D85E12) Rabbit mAb	Cell Signaling	#5558; RRID: AB_10013750
IRE1α (14C10) Rabbit mAb	Cell Signaling	#3294; RRID: AB_823545
GAPDH (6C5) mouse mAb	Santa Cruz	sc-32233; RRID: AB_627679
human TM6SF2 polyclonal rabbit Ab	This paper	N/A
phospho-IRE1α Ser724 polyclonal rabbit Ab	Novus Biologicals	NB100-2323; RRID: AB_10145203
IDE Polyclonal Rabbit Ab	Origene	TA327113; RRID: N/A
KDEL	Abcam	ab12223; RRID: AB_298945
Bacterial and virus strains		
Ad-GFP	This paper	N/A
Ad-TM6SF2	This paper	N/A
Ad-TM6SF2 E167K	This paper	N/A
Chemicals, peptides, and recombinant proteins		
Trypsin-EDTA solution 10X	Thermo Fisher Scientific	25300054
DPBS	Thermo Fisher Scientific	14040133
PhosStop phosphatase inhibitor	Roche	4906845001
cOmpleteTM protease inhibitor mixture	Roche	11836170001
RIPA Buffer (10X)	Thermo Fisher Scientific	89900
Methanol	Fisher Scientific	BPA4124; CAS 67-56-1
Ethanol	Fisher Scientific	AC615090040
Glucose	Sigma	G7021
Humulin R (Insulin)	Humulin	Humulin R U-100
DMEM, low glucose	Thermo Fisher Scientific	Cat# 11885084
DMEM, high glucose	Thermo Fisher Scientific	Cat# 11995065
Penicillin-Streptomycin	Thermo Fisher Scientific	Cat# 15070063
Protein A-agarose beads	Santa Cruz	sc-2001
TRIzol reagent	Thermo Fisher Scientific	15596026
SYBR Green Supermix	Bio-Rad	#1708880
Oil Red O	Sigma	O0625
Oleic acid	Cayman Chemical	90260
Critical commercial assays		
Blood glucose meter/strps	Contour	Contour next
RNeasy Mini Kit	Qiagen	Cat# 74106
SuperScript III	Thermo Fisher Scientific	18080051
Ultra-Sensitive Mouse Insulin ELISA Kit	Crystal Chem	#90080
Deposited data		
microarray analysis	GEO	GSE146146

(Continued on next page)

Continued

REAGENT or RESOURCE	SOURCE	IDENTIFIER
Experimental models: Cell lines		
Huh-7 cells	JCRB Cell Bank	JCRB0403; RRID: CVCL_0336
Experimental models: Organisms/strains		
Mouse: Wild type, Tm6sf2 KI mice, C57BL/6J background	This paper	N/A
Oligonucleotides		
Primers used for quantitative analysis, see Table S10	Sigma	N/A
Genotyping DNA primer for endogenous Tm6sf2 allele, forward, 5'- ATTCAGGCA GGCCAGGGTAAGGA-3'	Sigma	N/A
Genotyping DNA primer for endogenous Tm6sf2 allele, reverse, 5'- AAGAGCAGGG CAGCAAGGCAGACT-3'.	Sigma	N/A
Recombinant DNA		
TM6SF2-GFP	Origene	RG214298
TM6SF2-GFP-E167K	This paper	N/A
Software and algorithms		
affy Bioconductor package in R		https://bioconductor.org/packages/release/bioc/html/affy.html
GraphPad Prism 8.3.0	GraphPad	https://www.graphpad.com/scientific-software/prism/
METAL	PMID: 20616382	http://csg.sph.umich.edu/abecasis/Metal/
SAIGE v0.29.4.3	PMID: 30104761	https://github.com/weizhouUMICH/SAIGE
EZColocalization in Image J	PMID: 30361629	https://github.com/DrHanLim/EzColocalization
Original Code	Zenodo	https://doi.org/10.5281/zenodo.5508385

RESOURCE AVAILABILITY

Lead contact

Further information and requests for resources and reagents should be directed to and will be fulfilled by the lead contact, Y. Eugene Chen (echeum@umich.edu), Cardiovascular Center, Department of Internal Medicine, University of Michigan Medical Center, Ann Arbor, MI 48109, USA

Materials availability

All the plasmid generated in this study is available from the Lead Contact without restriction. For the Tm6sf2 KI mouse, please submit a Materials Transfer Form to the University of Michigan.

Data and code availability

- The raw microarray data has been deposited in the Gene Expression Omnibus (GEO) database: GSE146146.

- Software used for analysis is available from https://github.com/weizhouUMICH/SAIGE and https://genome.sph.umich.edu/wiki/METAL. Original code has been deposited at Zenodo and the DOI is listed in the key resources table.

- Any additional information required to reanalyze the data reported in this paper is available from the lead contact upon request.

EXPERIMENTAL MODEL AND SUBJECT DETAILS

Animals

Tm6sf2 (C>T variant) knock-in (KI) mice in the C57BL/6J background were generated with clustered regularly interspaced short palindromic repeat (CRISPR)/Cas9 technology (Fan et al., 2016). The guide RNA targeted the mouse *Tm6sf2* coding region sequence 5'- GTAAATACAGTTCAGAGATG*AGG* -3' was introduced with the Cas9 protein and a single strand DNA oligo containing the intended point mutation and a silent mutation on the *AGG* PAM sequence (AGG to AGA) as KI template. The genomic DNA containing the variant was amplified by polymerase chain reaction (PCR) with the following primers: forward, 5'- ATTCA GGCAGGCCAGGGTAAGGA-3'; and reverse, 5'- AAGAGCAGGGCAGCAAGGCAGACT-3'. The amplified DNA fragments (779 base pairs) containing the variant (C>T variant) were sequenced with the reverse primer. *Tm6sf2* KI mice and age-matched littermate wild type (Wt) mice on C57BL/6J background were fed a high-fat diet (HFD) (20% protein, 60% fat, 20% carbohydrate by calories; D12492, Research Diets, New Brunswick, NJ), or normal chow diet (22.5% protein, 11.8% fat, and 52% carbohydrate by mass) as indicated. Both male and female animals were used. All mice were maintained in a controlled environment at 22°C with a 12-hour light/dark cycle and had access to water and food ad libitum. All animal studies were approved in accordance with the University of Michigan Animal Care and Use Committee.

Cell lines and primary cultures

Huh-7 cells (RRID: CVCL 0336) were used in the study

Origin: Human hepatocyte-derived cellular carcinoma cell line.

Culture media and conditions: Huh-7 cells were cultured in Dulbecco's modified Eagle's medium (DMEM) supplemented with 10% fetal bovine serum, and 1 % penicillin-streptomycin in a 5% CO_2 atmosphere at 37°C. We did not authenticate this cell line in our laboratory.

Binary trait genetic association studies

Sex-stratified single variant association results under an additive model from European-ancestry samples in the DIAbetes Genetics Replication And Meta-analysis (DIAGRAM) consortium (effective N_{female}=96,460 and effective N_{male}=127,961) were used for type 2 diabetes (T2D) (Small et al., 2018). Association testing was also performed in the Nord-Trøndelag Health Study (HUNT) and the United Kingdom Biobank (UKB) for T2D, chronic liver disease without cirrhosis, ischemic heart disease (IHC), and myocardial infarction (MI). The Nord-Trøndelag Health Study (HUNT) is a population-based health survey conducted in the county of Nord-Trøndelag, Norway, since 1984 (See supplemental information). The European ancestry subset passing quality control (N=69,635) was analyzed with N_{female}=36,887 and N_{male}=32,748. The UK Biobank (UKB) is a prospective cohort with genetic and phenotypic data for 500,000 individuals (Bycroft et al., 2018). The white British subset (N=408,595) was analyzed with N_{female}=220,896 and N_{male}=187,699. HUNT phenotypes are defined as a customized collection of relevant ICD9/10 codes (Table S1), and UKB phenotypes are defined as groupings of ICD9/10 codes, known as phecodes (Wei et al., 2017) (Table S2). The sample sizes for phenotypes within these cohorts are in Table S3. Standard quality control for genotyping and imputation was performed in each cohort, and the single nucleotide polymorphisms of interest have expected quality metrics (Table S4).

Association analysis was performed on chromosome 19, specifically focusing on the missense variant of interest, rs58542926, using a mixed logistic model implemented in SAIGE v0.29.4.2 (Zhou et al., 2018). SAIGE uses a genetic relationship matrix from common variants (M_{HUNT}= 249,749 and M_{UKB}= 340,447 to account for population stratification and cryptic relatedness.

Combined and sex-stratified association analyses were performed in UKB and HUNT. The variant was tested under additive, dominant, and recessive models for all binary phenotypes (Tables S5–S8). Neither recessive nor dominant inheritance demonstrated optimal model fit or significant association consistently across the traits, so we moved forwards with an additive inheritance model, with accounts for both. In UKB, the binary outcome was tested using genotype array, birth year, and first five genetic principal components as covariates. In HUNT, batch, birth year and first four genetic principal components were used as covariates. In both studies, the combined association analysis included sex as a covariate. Inverse-variance

weighted fixed-effect meta-analysis was performed with HUNT and UKB summary statistics for rs58542926 using METAL (Willer et al., 2010) (Table S9).

Quantitative trait genetic association studies

The summary statistics for the BMI were acquired from the GIANT Consortium data bank (Pulit et al., 2019) and for glucose and insulin related traits from MAGIC (Dupuis et al., 2010; Mann et al., 2003). For the glycemic traits and blood lipids, the analysis was run separately for males and females in UKB and HUNT using a linear mixed model implemented in SAIGE under an additive model as described above. The cohort-specific summary statistics (Table S10) were combined using inverse variance weighted meta-analysis. HOMA2-IR and HOMA2-β were calculated in HUNT using the HOMA2 Calculator and fasting glucose and fasting C-peptide measurements (https://www.dtu.ox.ac.uk/homacalculator/) (Bethel et al., 2020).

The Nord-Trøndelag Health Study (HUNT)

The Nord-Trøndelag Health Study (HUNT) is a population-based health survey conducted in the county of Nord-Trøndelag, Norway, since 1984. Individuals were included at three different time points during approximately 20 years (HUNT1 [1984-1986], HUNT2 [1995-1997], and HUNT3 [2006-2008]). In total, DNA from 71,860 HUNT samples was genotyped using one of three different Illumina HumanCoreExome arrays (HumanCoreExome12 v1.0, HumanCoreExome12 v1.1 and UM HUNT Biobank v1.0). We excluded samples that failed to reach a 99% call rate, had contamination > 2.5% as estimated with BAF Regress, large chromosomal copy number variants, lower call rate of a technical duplicate pair and twins, gonosomal constellations other than XX and XY, or whose inferred sex contradicted the reported gender. Samples that passed quality control were analyzed in a second round of genotype calling following the Genome Studio quality control protocol described elsewhere. Genomic position, strand orientation and the reference allele of genotyped variants were determined by aligning their probe sequences against the human genome (Genome Reference Consortium Human genome build 37 and revised Cambridge Reference Sequence of the human mitochondrial DNA; http://genome.ucsc.edu) using BLAT. PLINK v1.90 was then used to exclude variants if their probe sequences could not be perfectly mapped, cluster separation was < 0.3, Gentrain score < 0.15, showed deviations from Hardy Weinberg equilibrium in unrelated samples of European ancestry with p-value < 0.0001), had a call rate < 99% or another assay with higher call rate genotyped the same variant. Ancestry of all samples was inferred by projecting all genotyped samples into the space of the principal components of the Human Genome Diversity Project (HGDP) reference panel (938 unrelated individuals; downloaded from http://csg.sph.umich.edu/chaolong/LASER/), using PLINK. Recent European ancestry was defined as samples that fell into an ellipsoid spanning exclusively European population of the HGDP panel. The different arrays were harmonized by reducing to a set of overlapping variants and excluding variants that showed frequency differences > 15% between data sets, or that were monomorphic in one and had MAF > 1% in another data set. The resulting genotype data were phased using Eagle2 v2.3.Imputation was performed on samples of recent European ancestry using Minimac3 (v2.0.1, http://genome.sph.umich.edu/wiki/Minimac3) and a merged reference panel that was constructed by combining the Haplotype Reference Consortium panel (release version 1.1) and a local reference panel based on 2,202 whole- genome sequenced HUNT study participants. We excluded variants with rsq < 0.3 resulting in over 24.9 million well-imputed variants for single variant association analysis.

Statistical analysis of genetic association studies

The calculation of the difference of effect size between male and female analyses was calculated as described by Winkler et al. (Winkler et al., 2017) and hypothesis testing performed with a two-sided p-value in R. Principal components analysis was performed in 63,681 samples in HUNT on quantitative and binary traits (except fasting glucose and HbA1C which greatly limited sample size) to determine the number of independent traits being tested. 8 components explained 99.5% of the variance. When considering the two related but excluded blood traits, we determined the number of independent traits tested to be 9. Considering association testing across traits in males and females as replication and testing for the difference in effect size between the sexes as 9 additional tests, we set a Bonferroni threshold of 0.05/18 (0.00277778) account for multiple testing.

METHOD DETAILS

Glucose tolerance test and insulin tolerance test

Glucose tolerance test and insulin sensitivity were measured in 14-week-old male *Tm6sf2* KI mice or 12 to 14-week-old female *Tm6sf2* KI mice on chow diet. Oral glucose tolerance test (OGTT) was performed in the *Tm6sf2* KI mice and Wt mice fasted for 5 h. At time 0, blood glucose was measured, and immediately after that, 2 g of glucose (dissolved in water)/kg body weight were delivered by oral gavage. Insulin tolerance test (ITT, 0.8 U/kg body weight, i.p.) was conducted in the mice fasted for 5 h.

Fourteen-week-old male *Tm6sf2* KI mice or twelve to fourteen-week-old female *Tm6sf2* KI mice and respective control mice were fed a HFD. ITT (fasted for 5 h, insulin 1 U/kg, i.p.) and OGTT (fasted for 5 h, glucose 1g/kg, gavage), were performed after 18-week HFD feeding in male mice or 20-week HFD feeding in female mice. Blood glucose was measured using a blood glucose meter (Contour Next) at the indicated time points.

Liver samples, plasma insulin measurement and Lipid Profiles

The liver samples for H&E, Oil Red O staining and phosphorylation of AKT and GSK3β, plasma insulin and lipid profiles including total cholesterol (TC), low-density lipoprotein cholesterol (LDL-c), high-density lipoprotein cholesterol (HDL-c), and triglyceride (TG) were measured after 20-week HFD feeding in male mice or 22-week HFD feeding in female mice. Mice were fasted 5 hours before sample collection. Plasma insulin and Lipids were measured with a Cobas Mira Plus chemistry analyzer (Roche Diagnostics, Indianapolis, IN) at the Michigan Diabetes Research Center Chemistry Laboratory (University of Michigan) in a double-blinded manner. The plasma insulin collected from mice fasted for 5 h was measure by Ultra-Sensitive Mouse Insulin ELISA Kit (Crystal Chem, #90080).

Quantitative PCR

Total RNA from the mouse liver was extracted using TRIzol reagent (Thermo Fisher Scientific) according to the manufacturer's instructions. RNA was reverse transcribed into cDNA with SuperScript III (Thermo Fisher Scientific) and random primers (Thermo Fisher Scientific). The abundance of transcripts was measured by a real-time PCR system (Bio-Rad) using SYBR Green Supermix (Bio-Rad). The relative expression for each gene of interest was normalized with the internal control, 18S. The primer sequences are shown in Table S11.

Western blot

Tissue extracts were prepared with RIPA lysis buffer (25mM Tris-HCl pH 7.6, 150mM NaCl, 1% NP-40, 1% sodium deoxycholate, 0.1% SDS) supplemented with a PhosStop phosphatase inhibitor and cOmplete™ protease inhibitor mixture (Roche). Protein extracts were resolved by SDS PAGE. Blots were incubated overnight at 4°C with antibodies against the following proteins (source, catalog number, and dilution of the antibody are given in parentheses): IDE (Origene, TA327113, 1:1000), LIPIN1 (Cell Signaling, #14906, 1:1000), IRE1α (Cell Signaling, #3294, 1:1000) , phospho-IRE1α Ser724 (Novus Biologicals, NB100-2323, 1:1000), AKT (Cell Signaling, #4691, 1:2000), phosphor-AKT Ser473 (Cell Signaling, #4060, 1:1000), GSK3β (Cell Signaling, #12456, 1:2000), phospho-GSK3β Ser9 (Cell Signaling, #5558, 1:1000), GAPDH (Santa Cruz, sc-32233, 1:2000). A polyclonal rabbit anti-human TM6SF2 antibody was raised against a peptide corresponding to the C-terminal 15 amino acids of human TM6SF2 CPPPSDPLALHKKQH (YenZym Antibodies, LLC, CA). After washing, membranes were incubated with an IRDye-conjugated IgG (LI-COR Biosciences, Lincoln, NE) secondary antibody diluted 1:5000 for 1 h. The intensity of the protein bands was quantified using an image processing program (LI-COR Biosciences, Lincoln, NE).

Immunofluorescence

Huh 7 cells were transfected with plasmid encoding Wt TM6SF2 fused with GFP (TM6SF2-GFP) or TM6SF2-GFP containing E167 variant. After 24 hours of transfection, cells were treated with ethanol (control) or OA (400 μm) for 18 hours. Cells were fixed and immunostained with anti-KDEL antibody (Abcam, ab176333, 1:200). Colocalization of TM6SF2-GFP and KDEL was quantified by Pearson's correlation coefficient (PCC) using Image J EzColocalization plugin.

Cell culture and oleic acid (OA) treatment

The human hepatocyte-derived cellular carcinoma cell line Huh-7 was cultured in Dulbecco's modified Eagle's medium (DMEM) supplemented with 10% fetal bovine serum, and 1 % penicillin-streptomycin in a 5% CO_2 atmosphere at 37°C. Upon 80% confluence, Huh-7 cells were infected with adenovirus (Ad) expressing human TM6SF2, TM6SF2-E167K knock-in (KI) mutant or green fluorescent protein (GFP) control, in combination with adenovirus expressing IRE1α at multiplicity of infection (MOI) of 100. Human IRE1α is a low abundant protein in Huh-7 cells. After infection, the Huh-7 cells were incubated with DMEM containing vehicle (PBS) or 400 μM oleic acid (OA) for 18 h to induce lipid accumulation *in vitro* (Moravcova et al., 2015).

Co-immunoprecipitation (Co-IP) analysis

Huh-7 cells were harvested and used for Co-IP with a rabbit polyclonal anti-IRE1α antibody (Cell Signaling, #3294), followed by immunoblotting with the anti-TM6SF2 antibody to detect the association between IRE1α and TM6SF2 in Huh-7 cells under the normal or lipid overload conditions. In brief, 300 μg of protein extracts were incubated with 20 μl of protein A-agarose beads, and 3 μg of anti-IRE1α antibody at 4°C for overnight with rotation. After centrifugation, the supernatant containing non-bound protein was removed, and the eluted proteins were separated by SDS-PAGE. The blots were incubated with anti-TM6SF2 antibody overnight at 4°C, then incubated with secondary antibody conjugated to horseradish peroxidase (1: 10,000) for 1 h at room temperature. Signals were detected using ECL Western Blotting Substrate on X-ray film.

Histology

The mouse liver sections were routinely counterstained with hematoxylin and eosin (H&E) staining and Oil Red O staining (ORO). For ORO, frozen liver sections (8 μm) were stained with 5% ORO (Sigma-Aldrich, St. Louis, MO) and then counter-stained with hematoxylin. Histological staining was performed by the *In Vivo* Animal Core at the University of Michigan. The H&E and Oil Red O sections were examined under light microscopy. A total of 6 tissue sections were analyzed for each animal.

Microarray analysis

The microarray analysis was performed by the DNA sequencing core at the University of Michigan. Briefly, RNA from the liver was extracted and hybridized on Human U133 Plus 2.0 GeneChips (Affymetrix) and then scanned using the Affymetrix 3000 7G GeneChip Scanner with Autoloader. Log2 expression values were calculated using RMA from the affy Bioconductor package in R.

QUANTIFICATION AND STATISTICAL ANALYSIS

Statistical analyses were performed using GraphPad Prism version 8.0 (GraphPad Software, San Diego, CA). Unless indicated otherwise, values are presented as mean ± standard error of the mean (SEM) showing all points. All data were tested for normality and equal variance. If the data passed those tests, Student t-test or two-way ANOVA with Bonferroni correction was used to compare two groups. One-way ANOVA followed by Bonferroni post hoc test was used for comparisons among >2 groups. If the data did not pass those tests, nonparametric tests (Mann-Whitney U or Kruskal-Wallis) were used. P-value < 0.05 was considered statistically significant. P values were shown on the figures as asterisks: *, $P < 0.05$; **, $P < 0.01$.